Structural complexity in grain boundaries with covalent bonding

E. Tarnow,* P. Dallot, P. D. Bristowe, and J. D. Joannopoulos
Massachusetts Institute of Technology, Cambridge, Massachusetts 02139

G. P. Francis and M. C. Payne
Cavendish Laboratory, University of Cambridge, Cambridge CB3 0HE, England
(Received 6 April 1990)

The structural properties of two short-period twist boundaries in germanium are explored using a state-of-the-art total-energy calculation. The structures of these boundaries are found to be very complex, with boundary bonds that are distorted and weak. These systems are found to exhibit a large degeneracy in the number of local energy minima. Thus the boundaries have difficulty in arriving at a locally ordered state. The situation may be unique to the *semiconducting twist* grain boundaries due to the inherent frustration present between the tendency to form directional bonds and the imposed twist geometry which makes the bond formation improbable. This study focuses on the energy, coordination, volume change, and electronic states characteristic of the local minima. A trend towards dimerization is found especially in the highest-angle twist boundary.

I. INTRODUCTION

Most materials of engineering and technological importance are polycrystalline. They consist of an aggregate of randomly oriented single crystals. The regions separating each single crystal are called grain boundaries. Grain boundaries influence the properties of polycrystalline materials in many significant ways. For example, they can be responsible for embrittlement, corrosion, fracture, polarization, and short-circuit diffusion.[1] In semiconductors, the electrical properties of thin polycrystalline films are important since these films are commonly used in device technology.[2] The presence of a grain boundary in an electronic device can degrade its performance by introducing enhanced resistance and capacitance effects. These effects are directly attributable to the intrinsic structural disorder of the grain boundary.

From a physics point of view, grain boundaries are interesting because, when compared to point or line defects, they represent a higher level of microscopic complexity. However, unlike amorphous materials, they have elements of order such as periodicity and a well-defined thickness. Some grain boundaries are more ordered than others. In terms of relative complexity, coherent twin boundaries are clearly more ordered than boundaries of an arbitrary misorientation and this is reflected in their physical properties, e.g., low energy and specific resistivity. Intermediate between these two geometrical extremes lie symmetrical tilt and twist boundaries. On the basis of the structural-unit model[3,4] and crystallographic considerations,[5] it is apparent that twist-boundary structures are generally more complex than those of symmetrical-tilt boundaries. Both kinds of boundaries can be manufactured and characterized at the microscopic level using x-ray diffraction[6] or high-resolution electron microscopy.[7] With the availability of new computational techniques[8,9] based on first-principles methods, it is now possible to predict and correlate with some accuracy the details of the atomic and electronic structures of these boundaries.

In this article, the phase space of two relatively short-period high-angle twist boundaries in germanium is explored using state-of-the-art quantum-mechanical methods. These methods are necessarily numerical since no theorem exists to predict the ground-state properties of a grain boundary. They involve an equation-of-motion method[10,11] to minimize to the total energy of the boundary using density-functional and pseudopotential theory.[12] A pure twist boundary is chosen for study since it represents a system of sufficient complexity to be interesting while at the same time it can be constructed with a relatively small unit cell to make the computational difficulties tolerable. Previous theoretical work on semiconductor grain boundaries using nonclassical methods has primarily focused on symmetrical-tilt boundaries or twin boundaries which have invariably exhibited tetracoordinated structures and well-defined energy minima.[13-19] The energies of [111] twist boundaries have also been computed previously but with little description of the relaxed structures.[20] Previous classical calculations, principally on metals,[21] but also on semiconductors,[22] have indicated that the energy surface of a pure twist boundary is less well defined than that of a pure tilt boundary for intrinsic geometrical reasons referred to above which are related to the local atomic arrangement and freedom for relaxation. A similar result is anticipated in the present study but may be further enhanced by the presence of realistic directional bonding and rehybridization effects that may reduce the ease with which atoms can rearrange. Subtle effects such as small bond-length and bond-angle distortions and interface states in the band gap may therefore be important. Germanium was chosen over silicon as the computational material mainly for technical reasons—a reliable *ab initio* local pseudopotential is available.[12] In addition, available experimental data indicate that grain boundaries in germanium and silicon are isomorphic.[23]

Due to the microscopic complexity of the grain boundaries to be considered, the investigation will yield an overall understanding of the system rather than specific results such as the absolute ground-state energy structure. However, statements will be made concerning the energy scales of the system, the nature of the local bonding, the presence of electronic states in the band gap, the local volume changes, and the breaking of symmetry. The present work represents the authors' current understanding of these grain boundaries and corrects our previous publications[8,24] which we found to contain numerical errors.[25] Experimentally, little is known about high-angle twist boundaries in semiconductors. The atomic structure of twist boundaries, in contrast to tilt boundaries, cannot be determined reliably using high-resolution electron microscopy.[26] Diffraction contrast effects in low-resolution experiments have demonstrated the stability of these boundaries in both silicon and germanium by observing the magnitude and direction of the Burgers vectors of the secondary grain-boundary dislocations.[27,28] The principal experimental problem has been preparing thin-film bicrystal specimens of controlled geometry which are free of impurities and other defects. The general properties of grain boundaries in semiconductors were reviewed by Grovenor[29] in 1985 and several conference proceedings provide more recent information.[30,31]

II. CRYSTALLOGRAPHIC ASPECTS OF TWIST-BOUNDARY STRUCTURE

This paper considers the structure of two short-period twist boundaries formed by bringing together the (001) faces of two diamond cubic semicrystals and rotating them about a [001] axis. Since the diamond lattice has a two-point basis, the origin for rotation about [001] can be either (0,0,0) or $(\frac{1}{4},\frac{1}{4},\frac{1}{4})$. As a consequence, a complete microscopic specification of the boundary requires the location of the boundary plane as well as the usual parameters describing the misorientation and relative translation of the crystals. Because of the cubic symmetry of the diamond lattice (space group $Fd3m$), all distinct [001] twist-boundary structures can be generated in the angular range $0 \le \theta \le 45°$ provided the origin of rotation is specified. If the boundary plane is kept fixed, then all distinct structures are generated in the range $0 \le \theta \le 90°$. A short-wavelength periodicity is introduced into the boundary when the misorientation angle takes certain singular values. This periodicity corresponds to that of the plane of the coincidence-site lattice[32] (CSL) which lies parallel to the boundary. A measure of the periodicity is the Σ index, the inverse density of coincidence sites. Because of the two-point basis of the adjoining lattices, two distinct coincidence-site patterns with the same Σ can be obtained for any given misorientation angle θ corresponding to rotations about the two different origins. The same patterns will be generated by rotations of $90°-\theta$ if the boundary plane is kept fixed. Once the angle of misorientation angle and boundary plane are chosen, then all local boundary structures constrained to this crystallography will be found by translation of the two crystals within the irreproducible zone of the unit cell of the pattern-conserving, or DSC (displacement shift complete), lattice.[32]

The specific twist boundaries to be investigated have the smallest possible value of Σ for the (001) system, i.e., $\Sigma=5$. In the present study, these boundaries are specified in terms of a fixed origin of rotation and, therefore, two misorientation angles, 36.9° and 53.1°, provide the desired structures. To be consistent with earlier work,[8,24] these boundaries are labeled $\Sigma5(36.9°)$ and $\Sigma5^*(53.1°)$. This distinction in notation is useful in discussing the different structural domains that may occur in the $\Sigma=5$ system. The unit-cell vectors of the CSL and DSC lattices in the plane of the boundary for both $\Sigma5$ and $\Sigma5^*$ are of the type $\frac{1}{2}a\langle 310\rangle$ and $\frac{1}{10}a\langle 310\rangle$, respectively, where a is the lattice constant. The unrelaxed CSL and DSC unit-cell structures for both boundaries are depicted in Fig. 1 and are body-centered tetragonal. The CSL cells are indicated by dashed lines. Four (004) planes are shown projected along [001] so that, in each case, two planes are above and two are below the boundary. It is seen that the two boundary structures are related by a 90° rotation of either the upper or lower crystals. Further examination shows that they are also related by an out-of-plane translation equal to $\frac{1}{20}a\langle 315\rangle$ which can be viewed as a transformation involving the removal or insertion of a (004) plane normal to one of the boundaries. Thus, despite their wide angular separation, it is conceivable that the $\Sigma5$ and $\Sigma5^*$ boundaries could coexist in domains bordered by steps and grain-boundary dislocations with Burgers vector $\frac{1}{20}a\langle 315\rangle$.

Classifying the twist boundaries in terms of their bicrystal symmetry elements is also important since symmetry can reduce the number of distinct structures that need to be considered and also indicate preferred structures through the principal of symmetry-dictated energy extrema. The space group of the pattern produced by the two rotated lattices completely specifies the translational and point symmetry of the unrelaxed twist boundaries. This pattern is called the dichromatic complex.[33] In their untranslated state, the structures shown in Fig. 1 for $\Sigma5$ and $\Sigma5^*$ have maximal symmetry and belong to the $I\bar{4}2'm$ and $I4_1/am'd'$ space groups, respectively.[34] Relaxations will, of course, modify these space groups. However, the properties of these symmetry groups can be used to determine, at least initially, that part of configuration space which contains all unique structures. In the plane of the boundary, this irreducible zone is found to be $\frac{1}{4}$ of the DSC unit cell and, therefore, only $\frac{1}{100}$ of the CSL unit cell. Figure 2 shows the DSC unit cells for both boundaries with the irreducible zones indicated by the shaded areas. The coordinates used to specify the size of the unit cells are based on a CSL vector equal to unity. Thus, (0.2,0) refers to $\frac{1}{10}a[310]$ in Fig. 2(b). The different symbols indicate symmetry-related positions and the circled symbols refer to structures that were computed. The absence of fourfold symmetry results in the generation of nonequivalent structures when translations are made along [310] and $[\bar{1}30]$. With a grid spacing of 0.05, it is seen that coverage of the irreducible for $\Sigma5$ requires only seven calculations whereas for $\Sigma5^*$ it requires nine.

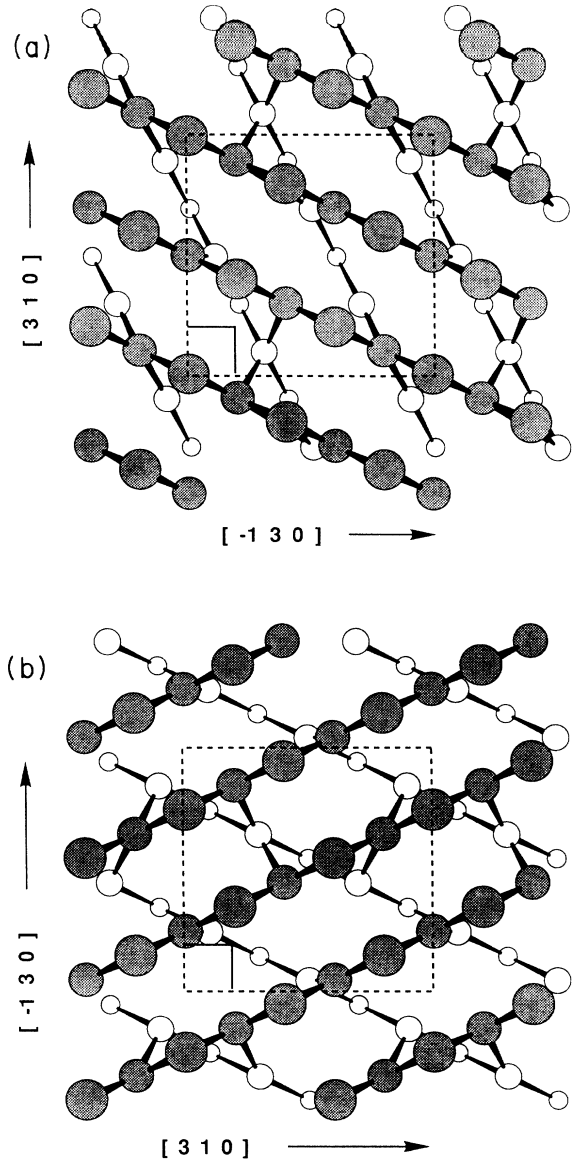

FIG. 1. Unrelaxed atomic positions in planes normal to the [001] direction for two twist boundaries in germanium: (a) $\Sigma5(36.9°)$ and (b) $\Sigma5^*(53.1°)$. Two layers above (solid circles) and below (open circles) the boundary plane are shown in both cases. The CSL unit cell is indicated by dashed lines and the smaller DSC cell is indicated by solid lines. Note that the x and y directions are reversed in (a) and (b), and that there is no relative translation of the upper and lower layers.

III. THE TOTAL-ENERGY METHOD AND RELAXATION STRATEGY

The total-energy calculations were made within the local-density approximation of density-functional theory using the exchange-correlation parametrization of Perdew and Zunger.[35] The pseudopotential approximation was utilized by employing a local Starkloff-Joannopoulos potential for germanium.[36] The scheme used to optimize the ionic and electronic structures was a modified Car-Parrinello algorithm[10,11] which employed plane waves up to an energy of 125 eV and two special **k** points at $(\frac{1}{4},\frac{1}{4},0)$ and $(-\frac{1}{4},\frac{1}{4},0)$. The computational cell, which extended periodically in all directions, consisted of two identical, but separate, twist boundaries related to one another by inversion symmetry. Each boundary was enclosed by two (004) layers of atoms that were free to relax and one further, outer layer that was kept frozen in the bulk position so as to emulate the bulk boundary condition. The atomic forces were relaxed until they were smaller than 0.1 eV/Å. The finite number of basis states used introduced a spurious internal stress known as the Pulay force.[37] This force, which was ignored in earlier work,[8,24] has been accounted for in the present study by adding a linear force correction. By estimating the errors due to every approximation used in the calculations, including finite **k**-point sampling, the model size, and the local pseudopotential, an overall error margin of 0.5 eV/unit-cell was determined. However, energy differences between different configurations should have significantly smaller error margins.

Since no optimization scheme is guaranteed to locate the absolute ground-state configuration, or even all possible metastable states, it is important to develop a systematic relaxation strategy which allows us to concentrate on the lowest-energy region of phase space. This is particularly true in the present study where the twist-boundary geometry exhibits a variety of bond-length and bond-angle distortions, where the bonding is directional and where the molecular dynamics algorithm used involves a rapid quench. In order to explore as much of boundary phase space as possible, a three-step relaxation

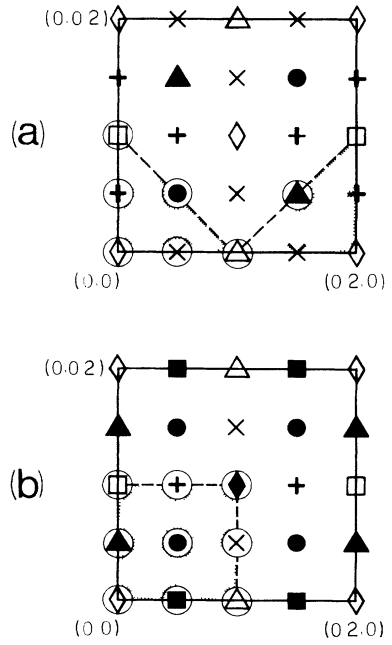

FIG. 2. DSC unit cells (solid lines) for (a) $\Sigma5(36.9°)$ boundary and (b) $\Sigma5^*(53.1°)$ boundary. The shaded areas indicated the irreducible zones for both boundaries. The coordinates are given as fractions of a CSL vector. Note that the x and y directions are reversed in (a) and (b) to be consistent with Fig. 1. The different symbols indicate symmetry-related positions and the circled symbols refer to structures that were computed.

process was initially used. As described later in Sec. IV D, the results of this process indicated that all possible geometries had still not been accessed, and further calculations were made. However, the initial three-step process involved the following: fixing the translation state at different positions within the irreproducible zone, and (1) determining the total energy by relaxing only the electrons, (2) determining the total energy by relaxing the electrons and the separation between the misoriented crystals (the local volume), and (3) determining the total energy by relaxing the electrons and all ion positions. The results of performing this sequential process are described in the following section.

IV. EQUILIBRIUM STRUCTURES AT FIXED TRANSLATION STATES

To illustrate the three-step relaxation process, attention is focused on the $\Sigma 5^*$ boundary. In subsequent discussion, however, the fully relaxed results for both twist boundaries are presented in detail.

A. Total energies

In the first step the total energies of the boundaries were determined by keeping the ions fixed in the translation states indicated by circled symbols in Fig. 2 and not allowing the local volume of the boundaries to change. The energy contour obtained in this calculation for $\Sigma 5^*$ is shown in Fig. 3. This contour map represents an extrapolation of the results so as to cover four DSC unit cells. It is seen that the energy range is about 10 eV with the minimum and maximum values equal to 17.3 and 27.4 eV/unit-cell,[38] respectively (1 eV/unit cell $\simeq 0.2$ J m^{-2}). The minima are located at $\frac{1}{20}a[\bar{1}30]$ [corresponding to position (0, 0.1) in Fig. 2(b)], in agreement with earlier work.[24] The large variation in energy arises from the close proximity of atom pairs for some translation states and not others. This is highlighted in Fig. 4 where the energy of each translation state is plotted against the distance of the two atoms that are closest across the boundary.

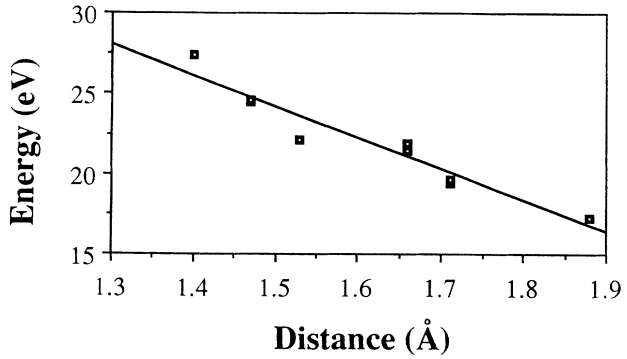

FIG. 4. Unrelaxed boundary energies of the nine translation states of $\Sigma 5^*$ as a function of the distance separating the two atoms of closest approach across the boundary.

In the second step the total energy of each boundary is minimized with respect to the distance between the misoriented crystals. This calculation is performed for each translation state but keeping the ions fixed within their planes. Thus, the minimum energy with respect to local volume is obtained. The resulting energy contour for $\Sigma 5^*$ is shown in Fig. 5 where it is seen that the location of the maxima and minima is not changed compared to Fig. 4, but that the variation in energy is *substantially* smaller. In addition, the absolute energies are considerably reduced with the minimum and maximum values equal to 9.4 and 9.9 eV/unit-cell,[38] respectively. Clearly, the high-energy interactions across the twist-boundary have been reduced by allowing the local volume to expand. At the same time, the distribution of distorted bonds no longer becomes highly dependent on translation state. This seems to be typical of twist-boundary geometries. The variation of boundary energy with volume expansion is shown in Fig. 6, where there is a clear correlation between increasing energy and expansion. Obviously, the lowest-energy structures have few atoms that are too close and they therefore require smaller volume change.

In the third step, the total energy of each boundary is

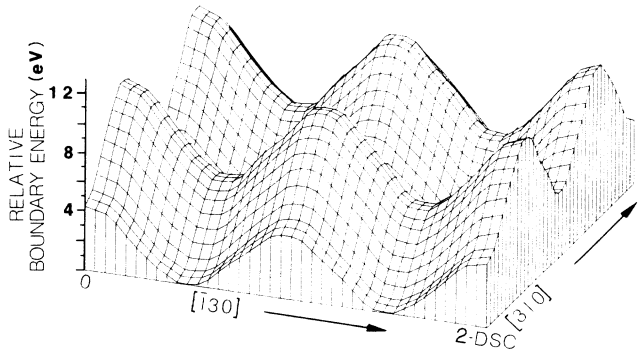

FIG. 3. The energy translation surface for the $\Sigma 5^*$ boundary before allowing any atomic relaxation. The surface covers four DSC unit cells and the boundary energy is normalized to the minimum which is located at $\frac{1}{20}a[\bar{1}30]$.

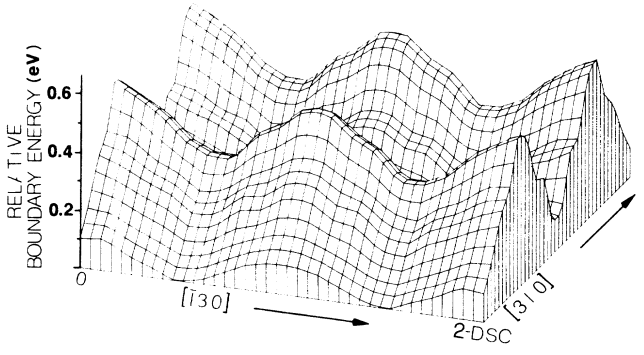

FIG. 5. The energy translation surface for the $\Sigma 5^*$ boundary after allowing the volume to expand. The surface covers four DSC unit cells and the boundary energy is normalized to the minimum, which is located at $\frac{1}{20}a[\bar{1}30]$. Note that the energy scale is much smaller than in Fig. 3.

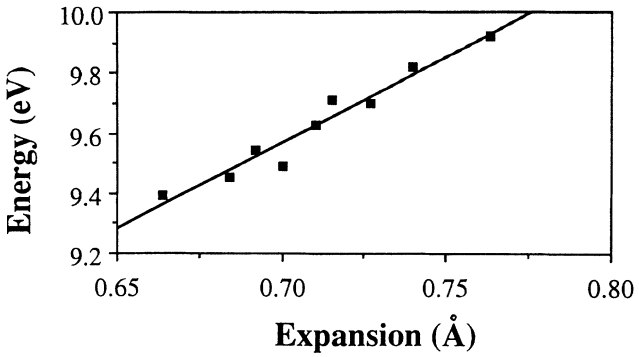

FIG. 6. Boundary energies of the nine translation states of Σ5* as a function of the local-volume expansion. No individual atomic relaxations were allowed.

minimized by allowing the ion positions to relax as well as the volume of the boundary region. The resulting total energies for Σ5 and Σ5* are given in Table I together with the corresponding translation states and volume expansions. The translation states are given as fractions of the CSL vectors in the boundary plane, e.g., for Σ5*, (0.1,0) represents $\frac{1}{20}a[310]$ and (0.1,0.1) represents $\frac{1}{10}a[120]$, as can be seen from Fig. 2(b). The energies are reported in eV/unit-cell and the volume changes are in Å/unit-area. The energies exhibit a number of important characteristics. First, for the Σ5* boundary, the local atomic relaxations have lowered the boundary energy by about 3 eV, which corresponds to 0.3 eV per boundary atom. This is a surprisingly small relaxation energy and is indicative of shallow bond minima. The energies are still all very similar with respect to translation state, but the minimum has now moved to the untranslated (0,0) position. The energies of the Σ5 boundary are comparable to those of the Σ5* boundary, but the minimum is located at the (0.05,0) position or $\frac{1}{40}a[\bar{1}30]$. The energy range for all translation states in the $\Sigma=5$ system is rather narrow (5.8–7.1 eV), resulting in an average boundary energy of about 6.5 eV/unit-cell.

B. Local volume changes

As can be seen from Table I, the fully relaxed volume changes for both the Σ5 and Σ5* boundaries are all positive and therefore represent expansions. The expansions corresponding to the minimum energy structures for Σ5 and Σ5* are 0.34 and 0.42 Å/unit-area, respectively. The average expansion for all structures is 0.25 Å/unit-area, with the deviation from this value being greater for Σ5* than Σ5. The boundaries expand, rather than contract, as a reaction to the presence of compressed bonds belonging to atoms that are in close proximity. This was also described to be the situation in step (2) of the relaxation process, but it is now seen that the expansions are smaller by a factor of 2. Clearly, the local rearrangement of atoms has resulted in the need for a smaller volume change. These local relaxations have also destroyed the strong correlation that existed between the boundary energy and volume expansion, as seen in Fig. 7, for both boundaries.

C. Local bonding

The atomic configurations resulting from the third step in the relaxation process are shown in Figs. 8 and 9 for the Σ5 and Σ5* boundaries, respectively. For the Σ5 boundary, seven configurations are shown corresponding to the seven circled translation states in Fig. 2(a). The

TABLE I. Twist-boundary energy (eV/unit-cell) and volume expansion (Å/unit-area) for the seven computed translation states of Σ5 and the nine computed translation states of Σ5*. The translation states are given as fractions of a CSL vector and are depicted as circled symbols in Fig. 2. The energies are displayed as columns in Fig. 11.

	Translation state (CSL vectors)	Energy (eV/unit-cell)	Volume expansion (Å/unit-area)
Σ5($\frac{1}{2}x[\bar{1}30], \frac{1}{2}y[310]$)	(0.0,0.0)	6.20	0.16
	(0.05,0.0)	5.79	0.17
	(0.01,0.0)	6.74	0.23
	(0.0,0.05)	6.35	0.23
	(0.05,0.05)	5.97	0.23
	(0.0,0.1)	7.04	0.28
	(0.15,0.05)	5.82	0.15
Σ5* ($\frac{1}{2}x[310], \frac{1}{2}y[\bar{1}30]$)	(0.0,0.0)	5.93	0.42
	(0.0,0.05)	6.28	0.07
	(0.0,0.1)	6.30	0.12
	(0.05,0.0)	7.02	0.40
	(0.05,0.05)	6.16	0.20
	(0.05,0.1)	6.32	0.12
	(0.1,0.0)	6.70	0.30
	(0.1,0.05)	6.83	0.23
	(0.1,0.1)	6.89	0.18

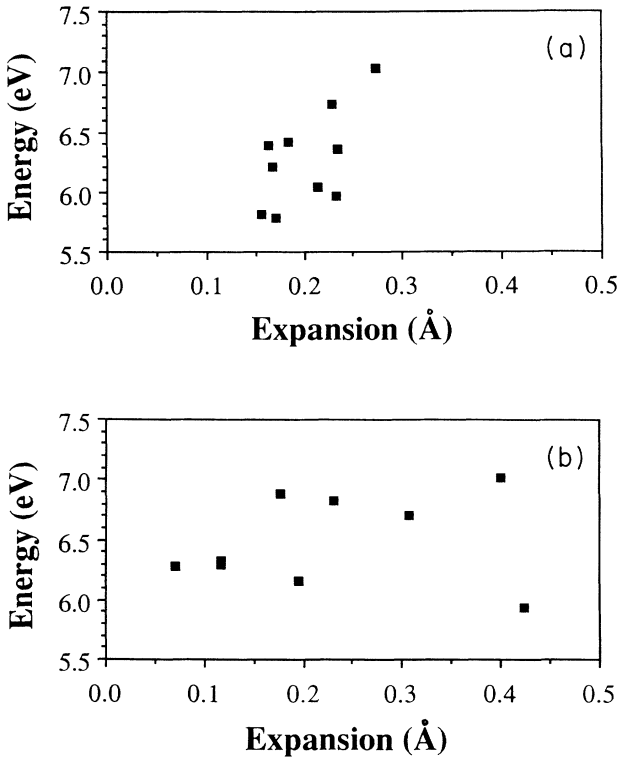

FIG. 7. Relaxed boundary energies of the translation states of (a) $\Sigma 5$ and (b) $\Sigma 5^*$ as a function of volume expansion. Volume changes and local atomic relaxations were allowed.

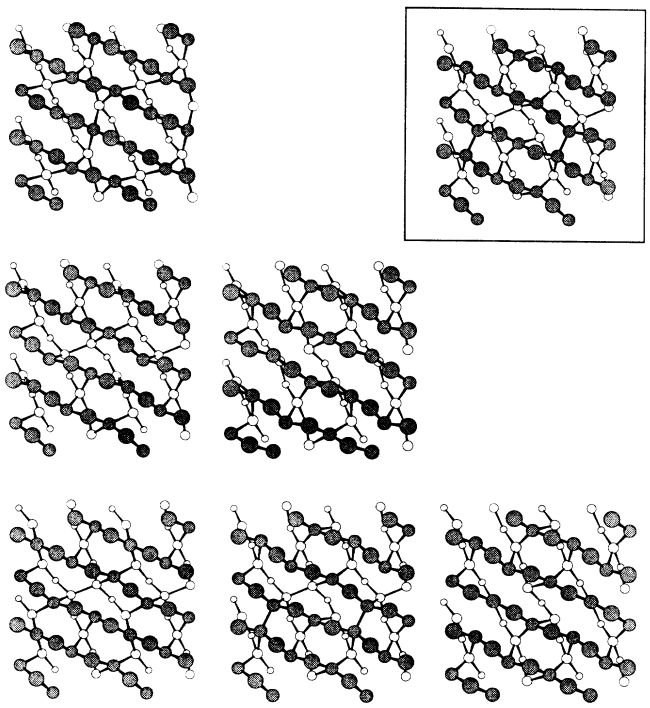

FIG. 8. Relaxed atomic configurations of the seven translation states of $\Sigma 5$ (36.9°). The orientation of the structures is the same as in Fig. 1(a). Their arrangement in the figure corresponds directly to the arrangement of circled symbols in Fig. 2(a) with the exception of the boxed structure, which corresponds to the state (0.15,0.05). Thus, the (0,0) state is the structure in the lower left-hand corner.

distribution of configurations is the same as the distribution of circled states with the exception of the boxed configuration which corresponds to the state (0.15,0.05). For the $\Sigma 5^*$ boundary, nine configurations are shown corresponding to the nine circled translation states in Fig. 2(b). For both boundaries, the untranslated (0,0) state is the configuration in the lower left-hand corner of Figs. 8 and 9. The number of atoms contained in the structures and their orientation is the same as in Fig. 1, i.e., four CSL unit cells viewed down [001] through the twist boundary. The criterion for drawing bonds between atoms is as follows: Atoms are bonded if their interatomic distance is equal to or less than 2.7 Å. This cutoff was chosen because the number of atoms with a bond length larger than 2.7 Å trails off rapidly and, as shown in earlier work[39] 2.7 Å corresponds to the limit beyond which the bond charge density between pairs of atoms changed from having one maximum to two separate maxima. Examination of the structures in Figs. 8 and 9 shows that they exhibit a variety of bond-length and bond-angle distortions and deviate from perfect tetrahedral coordination. For either boundary, no one particular structure dominates, although several of the structures have features in common. In general, there are two to four atoms per unit cell that are either over- or undercoordinated and four to six atoms that are fourfold coordinated, but with bond angles deviating from the perfect tetrahedral configuration. The average coordination number of the atoms in the $\Sigma 5$ boundary is 3.54, while it

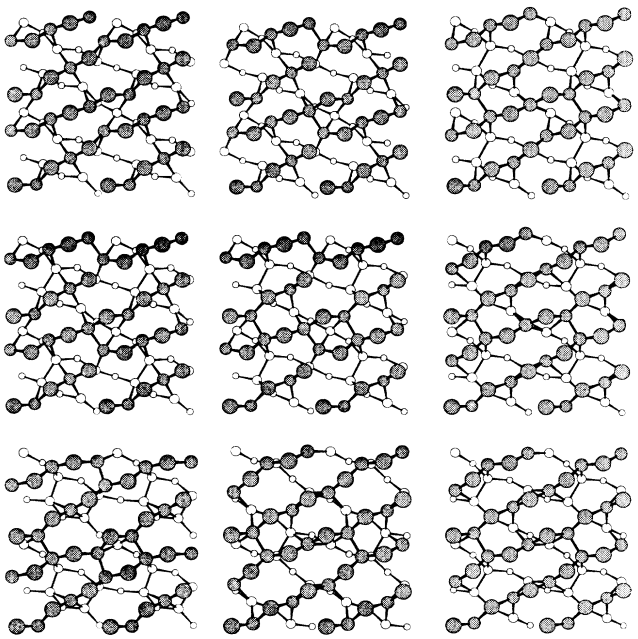

FIG. 9. Relaxed atomic configurations of the nine translation states of $\Sigma 5^*$ (53.1°). The orientation of the structures is the same as in Fig. 1(b). Their arrangement in the figure corresponds directly to the arrangement of circled symbols in Fig. 2(b). Thus the (0,0) state, which has the lowest energy, is the structure in the lower left-hand corner.

is 3.72 for the $\Sigma5^*$ boundary. There are two types of bonds at the boundary: those which cross the boundary and those which form $\langle 110 \rangle$ dimers along the surface of one of the grains. There are more dimerlike bonds in the $\Sigma5^*$ structures (1.9 bonds per configuration) than in the $\Sigma5$ structures (0.8). The number of intraboundary bonds is about the same for both boundaries: 6.7 bonds per configuration. Reviewing all the microscopic data obtained for both boundaries, it appears that the most significant structural feature distinguishing $\Sigma5$ and $\Sigma5^*$ is the tendency for $\Sigma5^*$ to form more $\langle 110 \rangle$ dimers. These dimers are similar to those found on the (001) free surface.[40] From this result, it is tempting to speculate that high-angle twist boundaries contain more dimer bonds than low-angle twist boundaries which may be comprised of all interboundary bonds. In particular, it is possible to build a model of a 90° boundary which is all dimerized, where the dimers of one surface fit nicely into the pattern of dimers on the opposite surface.

Figure 10(a) illustrates an average radial distribution function for the $\Sigma=5$ twist-boundary system obtained from all the $\Sigma5$ and $\Sigma5^*$ structures computed. Two curves are shown, one for the atoms in the first layer adjacent to the boundary (solid line), and the other for atoms in the second layer adjacent to the boundary (dashed line). It is seen that the curve for atoms in the second layer exhibits distinct peaks at the crystalline neighbor distances, implying that these atoms are in bulklike environments. However, the curve for atoms in the first layer has fewer and smaller peaks than in the second layer which implies that these atoms are in a more disordered environment. In fact, this curve is very similar to that obtained experimentally[41] for amorphous germanium as can be seen in Fig. 10(b). In particular, the experimental curve, shown dashed, and the computed curve has characteristically a well-defined nearest-neighbor peak and a missing third peak. The disorder at the boundary appears to be slightly greater than that of amorphous germanium, as indicated by the presence of a few configurations around 3 Å. Finally, we note that the choice of 2.7 Å as a bond-length cutoff is consistent with the dip in the radial distribution function at 3 Å.

The presence of a variety of bond distortions in all the calculated structures reflects the compromises that have been made in minimizing the total energy of a system that is constrained by rotation and translation. These compromises have resulted in boundary structures that all have quite similar energy with respect to translation state. It has been argued previously from classical calculations[21,22] that this may be expected for twist boundaries comprised of several atoms per lattice plane since, in such cases, approximately equal numbers of new bonds form as do break. In the present study, the additional effects due to electronic relaxation appear to enhance this result rather than suppress it.

D. The multiplicity of local minima and selecting a low-energy phase-space region

Let us now reconsider the question related to achieving a global minimum. Have we, in our calculations thus far,

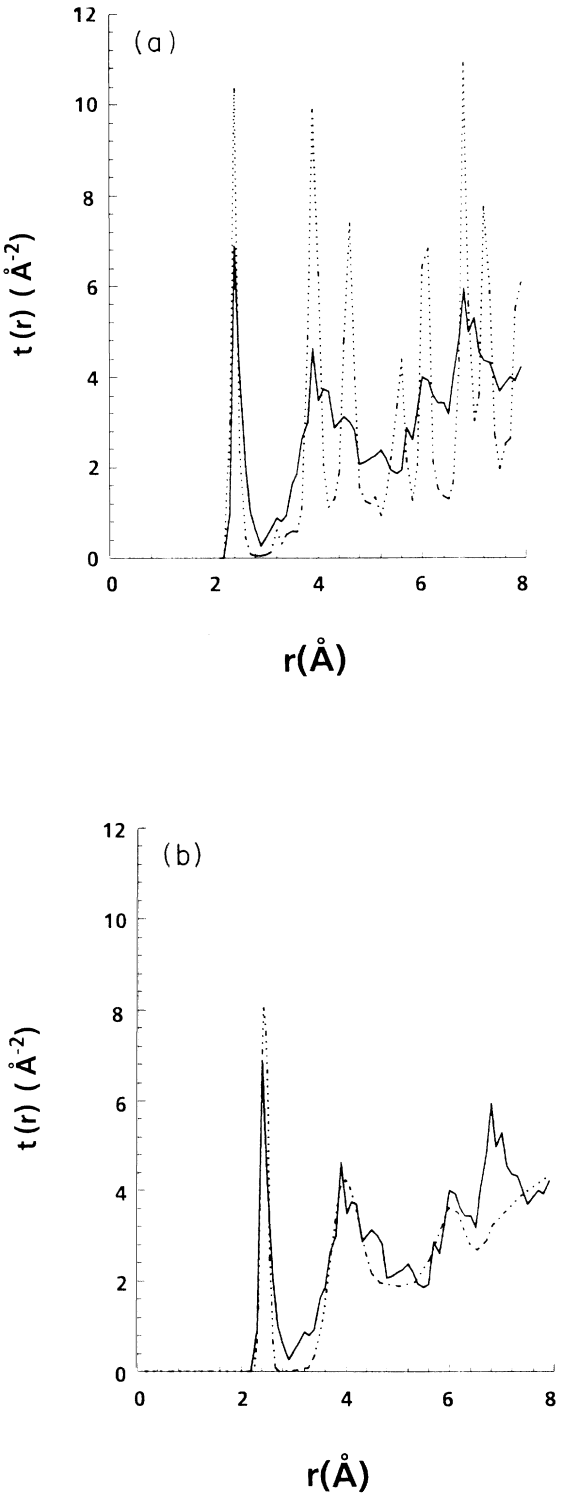

FIG. 10. (a) Average radial distribution function of the $\Sigma=5$ twist-boundary system for atoms in the first layer adjacent to the boundary (solid line) and the second layer adjacent to the boundary (dashed line). (b) Average radial distribution function of the $\Sigma=5$ twist-boundary system for atoms in the first layer adjacent to the boundary (solid line) compared to the experimental (see Ref. 41) distribution function for amorphous germanium (dashed line).

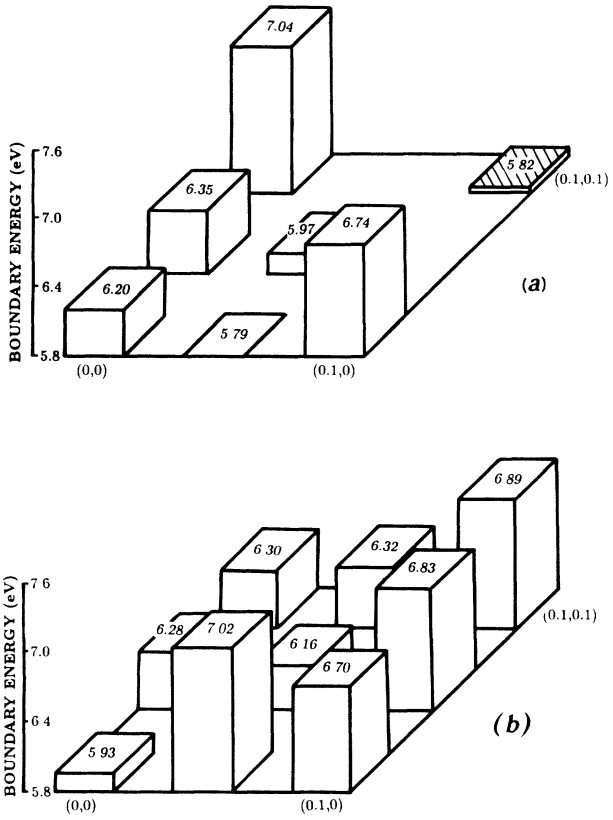

FIG. 11. Total energies, given in Table I, displayed as columns within the irreproducible zone of the DSC lattice for (a) $\Sigma 5$ and (b) $\Sigma 5^*$. The arrangement of columns corresponds directly to the arrangement of circled symbols given in Fig. 2 and to the arrangement of structures given in Figs. 8 and 9. Thus, the shaded column shown in (a) corresponds to the boxed structure in Fig. 8.

really reached the true ground state? We would have been reasonably confident had all the configurations we obtained looked very similar: This would have allowed us to conclude that there was only one minimum in phase space; we could then draw a total-energy surface as a function of translation state, identify the minimum and claim that it was the ground state. However, the situation we have arrived at is much more complex: The configurations we obtained are related to *different* minima; for example, some of the boundaries are dimerized while others are not. To emphasize this point, we display the energies for the different translation states as isolated columns in Figs. 11(a) and 11(b), rather than a continuous surface.

To truly identify the ground-state configuration, we would have to consider all of phase space. For the system at hand, this would be impossibly complex and time consuming. What we *can* do, however, is to use our data to select and focus on what appear to be low-energy regions of phase space, and investigate the local minima in these regions further. We do this for the $\Sigma 5^*$ boundary as follows.

For the $\Sigma 5^*$ geometry, a signature of a low-energy region appears to be dimer formation along the surfaces of the grain boundary. We attribute this to the fact that bonds across the boundary became more and more strained as we increased the twist angle rotation and that atoms would prefer to bind along each surface. Thus, with this in mind we are going to constrain our search in phase space to all structures that are maximally dimerized. Specifically, we will dimerize each individual surface, change the intersurface configuration by a relative translation, and the new configuration will be a new initial geometry from which we will apply a quench.

This procedure turns out to generate more geometries than expected. Naively, one might expect that translating the dimerized surfaces by one DSC vector would result in the same intersurface configuration. But this actually does not occur due to the presence of symmetry breaking.

As soon as the grain-boundary atoms start to relax, they can break the symmetries of the initial, unrelaxed, structure. The relevant type of symmetry breaking occurs when two atoms that originally occupied symmetry equivalent positions, to within a *translation by one or more DSC lattice vectors*, cease to do so. In the unrelaxed $\Sigma 5^*$ (0.0,0.0) boundary [Fig. 1(b)] there is only one nonequivalent atom in this sense (as we translate the grains throughout the DSC cells, the atomic identities are simply permuted). For the corresponding relaxed configuration (Fig. 9), there are five nonequivalent atoms. This type of symmetry breaking greatly enlarges the low-energy regions of phase space that we can consider. The unit cell of translations is no longer the DSC cell of the unrelaxed boundary. For example, if we rigidly translate the relaxed $\Sigma 5^*$(0.0,0.0) boundary (Fig. 9) by a DSC vector, we obtain a nonequivalent configuration. In fact, since there are 25 DSC unit cells per CSL unit cell, *there are 25 possibly nonequivalent configurations for this boundary geometry.* Figure 12 illustrates, in a schematic way, how transitions are made between the various

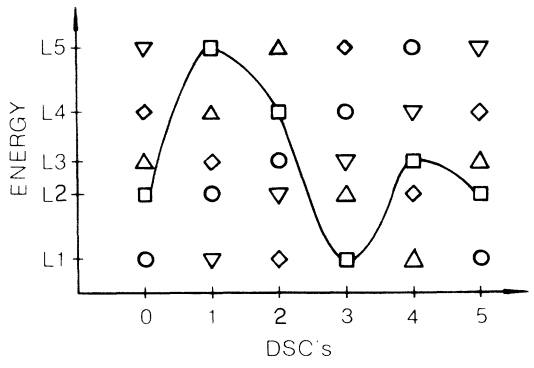

FIG. 12. Schematic energy-level diagram for a set of five grain-boundary geometries as a function of translations across a multiple number of DSC unit cells. The symbols identify how the geometries transform into each other. Note that the geometries transform back into themselves only after a CSL translation (five DSC translations).

grain-boundary configurations as several DSC unit cells are traversed. In this example, L1–L5 represent the energy levels of a set of five different grain-boundary geometries. For each geometry, translation by one to four DSC cells will generate the other members of the set. The symbols identify how the five different geometries transform into each other. Thus, the geometry with energy L2 at 0 DSC, transforms to geometries L5, L4, L1, and L3 after translation by one, two, three, and four DSC's, respectively.

The details and results of our calculations using this extended region of phase space are presented in the next section.

V. A CONTINUOUS TOTAL-ENERGY SURFACE

In this section the results of performing the fourth and final step in the relaxation process is described in which the minimum-energy structures obtained previously are rigidly translated beyond the irreproducible zone of the DSC unit cell and rerelaxed. The objective is to determine whether any new stable or metastable structures may be found by starting from a variety of different bonding configurations. Due to computational time constraints, this study was performed more thoroughly for the maximally dimerized $\Sigma5^*(0,0)$ boundary than for the $\Sigma5$ boundary. The size of the region beyond the irreproducible zone that may need to be examined cannot exceed the area of the CSL unit cell in the boundary plane. In fact, the symmetry of the relaxed $\Sigma5^*$ (0,0) boundary indicates that, at most, one-quarter of the CSL unit cell needs to be covered. [The translation state (x,y) is equivalent to the translation states $(0.2-x, y)$, $(x, -y)$ and $(0.2-x, -y)$]. We found that sufficient accuracy would be obtained if the new translation zone was sampled every 0.125 CSL vectors (or $\frac{1}{16}a\langle 310\rangle$). Thus, 16 new calculations were performed corresponding to translation states outside the original irreproducible zone. Figure 13 shows the result of an exploratory calculation

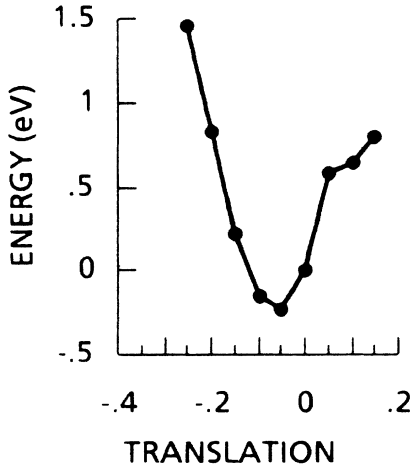

FIG. 13. The relative energy of the $\Sigma5^*(0,0)$ structure as it is translated along [310]. Translations are given as fractions of the CSL vector.

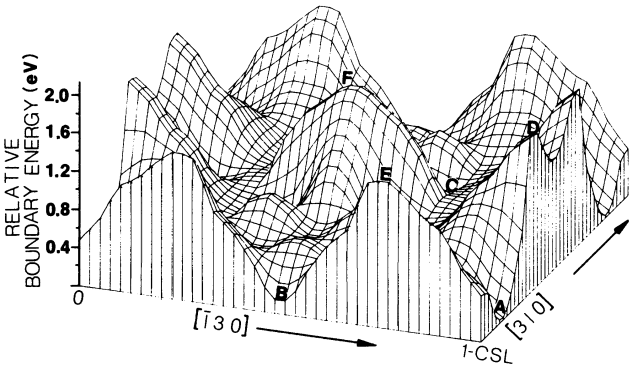

FIG. 14. The energy translation surface for the $\Sigma5^*(0,0)$ boundary obtained by performing extended translations beyond the DSC unit cell. The surface spans one complete CSL unit cell $[(x,y)$: $0.1<x<1.1, 0.<y<1.0]$ and was obtained by a mapping of the computed zone ($\frac{1}{4}$ of the CSL cell) into the rest of the cell. The locations of the three lowest energies are labeled *A*, *B*, and *C*, and the three highest energies are labeled *D*, *E*, and *F*. The boundary energy is normalized to the minimum, which is location *A*.

in which the $\Sigma5^*(0,0)$ relaxed structure is translated along [310]. It is seen that the variation in total energy [which is shown relative to the (0,0) state] is harmonic on a length scale of about 0.4 CSL vectors ($\frac{1}{5}a[310]$), that it is not periodic in the DSC lattice (0.2 CSL vectors), and that the minimum shifts slightly to $(-0.05,0)$, i.e., $-\frac{1}{40}a[310]$. Thus, this initial procedure has located a configuration of marginally lower energy than was obtained originally.

Figure 14 shows the final energy contour for the $\Sigma5^*(0,0)$ boundary. The energy range is about 1.7 eV with the minimum and maximum values equal to 5.7 and 7.4 eV/unit-cell, respectively. The contour spans one complete CSL unit cell and was obtained by a symmetry mapping of the computed translation zone ($\frac{1}{4}$ of the CSL cell) into the rest of the cell. It is found to have three local energy minima (located at points *A*, *B*, and *C*) and

TABLE II. Twist-boundary energy (eV/unit-cell) and volume expansion (Å/unit-area) for the three $\Sigma5^*$ structures of lowest and highest energy after extended translations beyond the DSC cell are made. The translation states are given as fractions of a CSL vector and are labeled *A*–*F* in Fig. 14.

	Translation state ($\Sigma5^*$ CSL vectors)	Energy (eV/unit-cell)	Volume expansion (Å/unit-area)
		Minima	
A	(0.25,0.0)	5.72	0.47
B	(0.1,0.5)	5.85	0.56
C	(0.475,0.375)	5.96	0.44
		Maxima	
D	(0.45,0.0)	7.38	0.46
E	(0.1,0.25)	7.29	0.42
F	(0.6,0.5)	7.35	0.70

three local energy maxima (located at points D, E, and F). The absolute minimum is point A corresponding to the $-\frac{1}{40}a[310]$ state [or equivalently $(-0.05,0)$, which is the same as (0.25,0)]. The contour is clearly not periodic with the DSC lattice. For example, points A and D are separated by a DSC vector, and yet they are relative minima and maxima in energy and correspond to quite different local structures. This dramatically illustrates the effect of starting the calculation with different local-bonding configurations which do not relax to the same structure despite the fact that the two grains in each case are in equivalent translational positions. The total energies, volume expansions, and translation states of all the minima and maxima are given in Table II. The corresponding atomic configurations are shown in Fig. 15 for both the minima (left panel) and for the maxima (right panel). The lowest-energy structure is located at the top of the left panel. It is noted that one of the minima (bottom left panel) is fourfold coordinated and that all the high-energy structures have atoms in close proximity across the boundary.

A further interesting result of the above calculations is shown in Fig. 16. This shows two relaxed structures of the (0.05,0) state (or $\frac{1}{40}a[310]$) resulting from initial configurations which were either the rigid-body geometry [Fig. 16(a)] or a geometry obtained by relaxing the (0,0) state and translating to (0.05,0) [Fig. 16(b)]. It is seen that the different initial bonding configurations yield similar structures, although Fig. 16(b) is fully dimerized, whereas Fig. 16(a) is not. The relative energies of the two structures are plotted on Fig. 17, which shows that the fully dimerized structure has the lower energy. Also shown in Fig. 17 is the energy path connecting the two structures which was obtained by a linear transformation of the atomic coordinates of one structure into the other structure. It is found that an energy barrier of about 0.1 eV separates the two structures which may suggest that they can coexist. A similar example of this phenomenon was found when performing additional translational calculations on the $\Sigma 5$ boundary. Figure 18 shows a characteristic group of atoms that form part of two different translation states of the $\Sigma 5$ boundary that are symmetry equivalent but yielding different configurations. The difference is an ammonia molecule-like inversion of a threefold center as highlighted in the figure. The energy barrier separating the two configurations is found to be $\simeq 0.05$ eV. The existence of an energy barrier and the

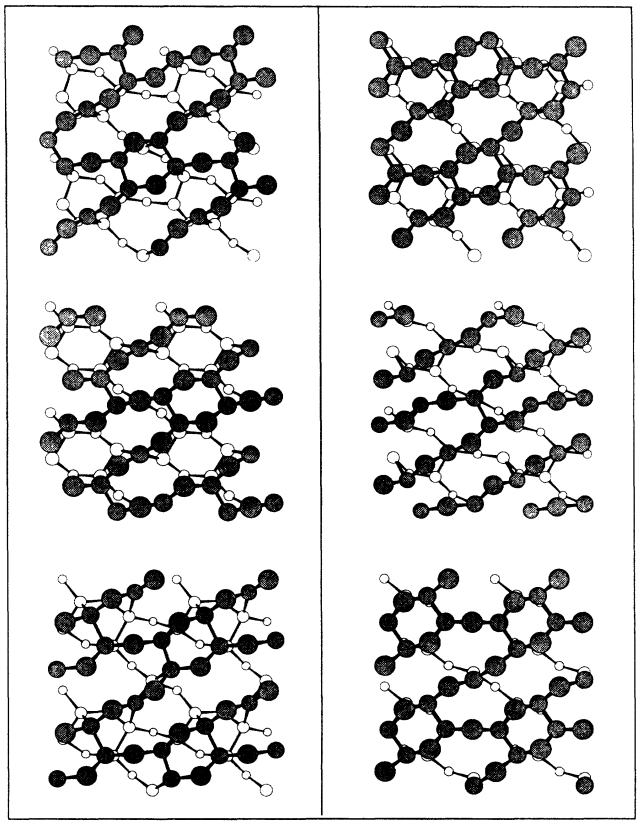

FIG. 15. Relaxed atomic configurations corresponding to the energy extrema $A-F$ in Fig. 14. The three minima A, B, and C, and the three maxima D, E, and F are shown top to bottom in the left- and right-hand panels, respectively.

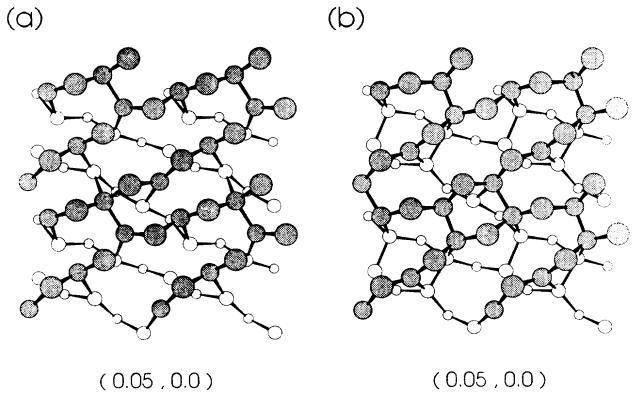

FIG. 16. Two relaxed atomic configurations of the (0.05,0) or the $\frac{1}{40}a[310]$ state of $\Sigma 5^*$. (a) was obtained from relaxation of the rigid-body geometry and (b) was obtained by translating the relaxed (0,0) state to (0.05,0) and rerelaxing.

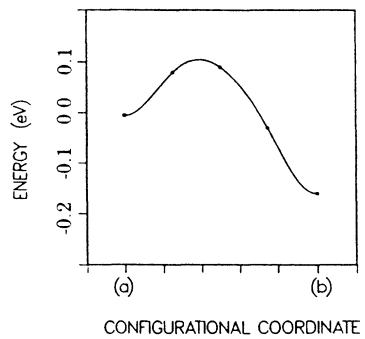

FIG. 17. Relative energy path connecting the two structures shown in Figs. 16(a) and 16(b).

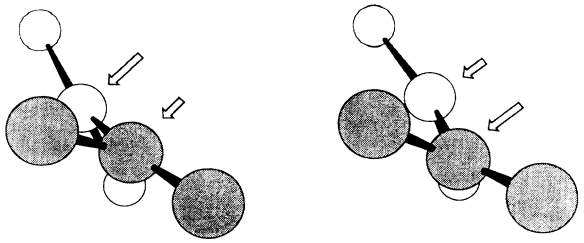

FIG. 18. Characteristic group of atoms that form part of two different translation states of Σ5 that are symmetry equivalent, but yield different configurations. The arrows highlight the differences.

similarity in boundary energies suggests that these configurations may be considered as tunneling states.

VI. GRAIN-BOUNDARY STATES IN THE BAND GAP

Since all the relaxed twist-boundary structures exhibit distorted or broken bonds, electronic states should be present in the band gap. The boundaries are thus expected to be intrinsically active electrically[42] (at least in the absence of passivative impurity elements) which has important technological consequences. To determine the presence of grain-boundary states, the electronic eigenvalues of the two lowest-energy Σ5 and Σ5* structures have been calculated at the $(\frac{1}{4},\frac{1}{4},0)$ **k** point. Figure 19 shows the presence of several energy states distributed throughout the band gap for both boundaries as expected. These are all *unfilled* states. The (a) and (b) labels refer to the Σ5* structures and the (c) and (d) labels to the Σ5 structures. It is seen that for the Σ5* structure labeled (a), a state exists below the top of the valence band (TOV) which implies, in this case, that the boundary would be charged. Further confirmation of the electrical activity of these low-energy structures has been obtained by computing the local density of states (LDOS) on each atom in the four layers adjacent to the boundaries. Figure 20 shows a typical result for a Σ5* structure. In the top panel of Fig. 20, the LDOS *relative to the bulk* on an atom in the first layer adjacent to the boundary is shown. In the lower panel, an atom in the second layer is considered. It is seen that the LDOS exhibits perturbations in the band gap for atoms in both layers although the perturbations are larger in the first layer. This result is consistent with the general distribution of distorted bonds in the boundary as described earlier.

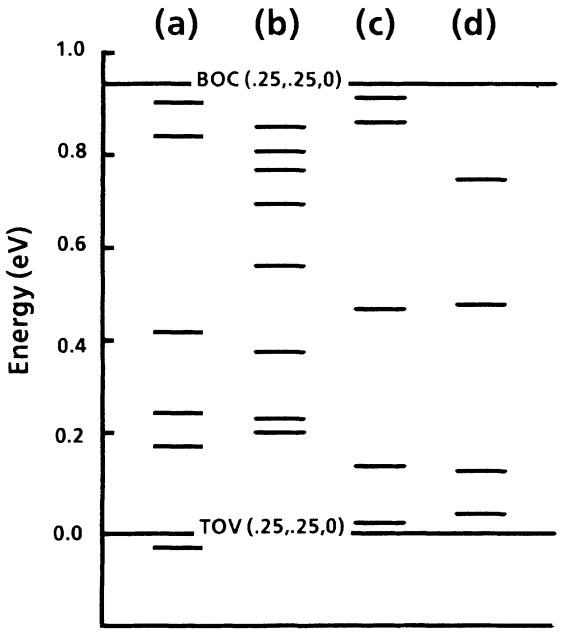

FIG. 19. Lowest-energy *empty* electronic states of the two lowest-energy Σ5* structures (a) and (b) and the two lowest-energy Σ5 structures (c) and (d). BOC and TOV refer to the bottom of the conduction band and top of the valence band of bulk Ge at the $(\frac{1}{4},\frac{1}{4},0)$ **k** point, respectively.

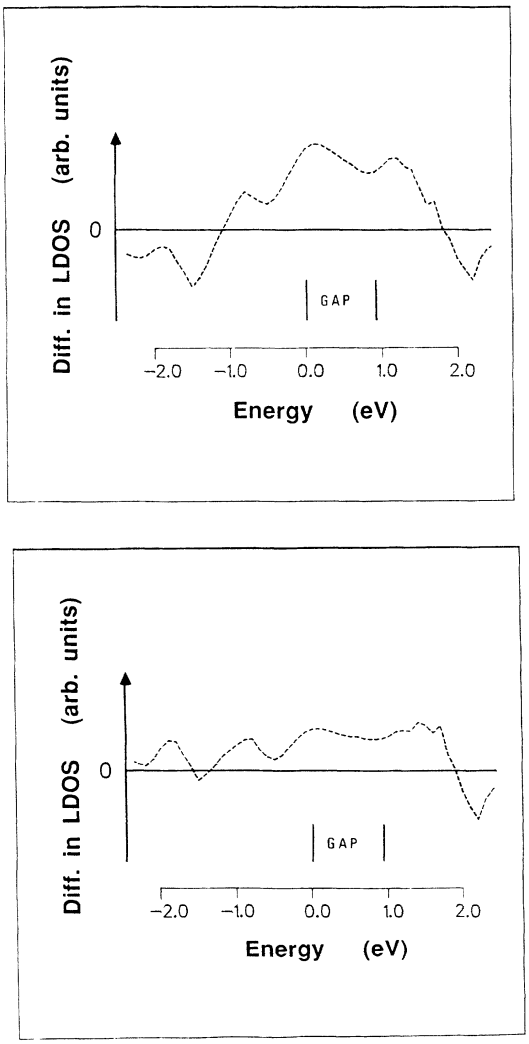

FIG. 20. Typical local density of states (LDOS), relative to the bulk, on an atom in the first layer adjacent to a Σ5* boundary (top panel) and on an atom in the second layer adjacent to the boundary (bottom panel).

VII. ADDITIONAL MODES OF RELAXATION: RECONSTRUCTION AND POINT DEFECTS

Since surfaces are known to relax by reconstructing to form larger unit cells, it is conceivable that grain boundaries may do the same thing. In fact, such an effect has already been observed experimentally for tilt boundaries in germanium.[43,44] For $\Sigma=5$ twist boundaries, therefore, it is possible that the preferred unit cell may contain ten or more atoms per lattice plane instead of five. Unfortunately, current computational resources prohibit testing such a model using total energy methods. However, some inferences may be made from the present results. The lowest-energy structure for the $\Sigma5^*$ orientation had a pronounced tendency to form dimerized bonds along the boundary plane. In order to dimerize all the atoms in the boundary plane, there must be an even number of atoms per unit cell. Thus, a (2×1) reconstruction for the $\Sigma5^*$ boundary is a possible candidate for a preferred structure. In order to test for energetically preferred reconstructions, a number of classical calculations were performed on the $\Sigma5^*$ boundary using the Stillinger-Weber potential[45] for silicon. In these calculations, the nine different translation states of the boundary were statically relaxed using a model containing four CSL unit cells. It was found that two of the nine translation states, (0.05,0) and (0.1,0) did reconstruct to form larger unit cells, namely $(\sqrt{2}\times\sqrt{2})$ and (2×1), respectively. However, both reconstructions were of relatively high energy and did not dimerize all the atoms in the boundary plane. It would thus appear that a low-energy (2×1) reconstruction with complete dimerization is not energetically preferred, at least using the Stillinger-Weber potential. This provided additional support for the approach used in the *ab initio* calculations which employed just one CSL unit cell. Of the remaining seven translation states that did not reconstruct, five were remarkably similar in structure to those obtained in the total energy calculations. However, it was found that the topology of the energy-translation surface was rather different from the total-energy result with the minimum located at (0,0.1) instead of (0,0).

Many of the initial bonding configurations used in the present study have involved atoms in close proximity across the boundary and are consequently in energetically unfavorable situations. Although these situations can be relieved by allowing in-plane translations and volume expansions, it is recognized that creating vacancies may accomplish the same result. Indeed, results of a calculation including one vacancy show that a drop in energy, comparable to that found for translations, is obtained.

The details of this calculation are as follows: The vacancy geometry was constructed by considering the unrelaxed configuration with the largest energy (corresponding to the energy peak in Fig. 3), and removing one atom from one side of the boundary that was "colliding" with the corresponding atom on the other side of the boundary. Total energies were then calculated using the three-step relaxation scheme discussed earlier. The results are 9.5 eV for purely electronic relaxation, 9.3 eV for electronic and local volume relaxation (the width increased by 0.20 Å with respect to bulk Ge), and 6.64 eV for electronic and complete ion relaxations (the width *decreased* by 0.07 Å with respect to bulk Ge). Thus, by removing one of the two atoms that were in very close proximity, the width of the boundary becomes smaller than before. Moreover, the energy of the vacancy boundary is very similar to the boundaries *without vacancies*. This result leads to the conclusion that the $\Sigma5^*$ boundary can absorb vacancies and interstitials without much change in energy. It also suggests that a $\Sigma=5(001)$ boundary may, in general, consist not only of $\Sigma5$ or $\Sigma5^*$ boundaries (that are related by a removal of a full layer of atoms),[27] but also all other boundaries that can be constructed by removal or insertion of single atoms. Furthermore, it opens up the possibility that the grain boundary can absorb not only single atoms or vacancies, but also dislocations resulting in boundary steps. The global structure of a $\Sigma=5(001)$ system may, however, be even more complex than this since the current calculations have suggested a multiplicity of metastable states separated by energy barriers. The overall structure, therefore, may contain not only dislocations but a network of different structural units.

VIII. FINAL REMARKS

From this investigation emerges one fundamental result: The microscopic properties of $\Sigma5$ and $\Sigma5^*$ twist boundaries are complex. Accordingly, it is difficult to distill simple physical models of the system and it is impossible to determine the absolute ground-state structure since the computed energy differences between the various metastable structures is so small. Nevertheless, it is possible to describe the types of configurations that constitute low-energy structures and their properties in terms of energy, symmetry, electronic states, local volume changes, and bonding characteristics.

Two major features contribute to the observed structural complexity: the intrinsic geometry of a twist boundary and the presence of strong directional bonding. The twist boundaries studied here involved many competing interatomic interactions, some favoring bond formation, others not. When this is coupled with covalent bonding, which restricts atomic relaxation, the result is a boundary-energy surface that is not highly dependent on translation state. Thus, many configurations are found within a few tenths of an eV/unit-cell and the local-volume changes do not correlate well with the boundary energy. Covalent bonding also causes a lowering of the boundary symmetry after relaxation which indicates that additional structures may be found if translations beyond the DSC unit cell are imposed on the relaxed boundaries. New structures are indeed found when this procedure is performed. It is emphasized that these extended translations do not change the fundamental properties of the DSC lattice. They are considered as a computational mechanism for generating alternate local bonding geometries. They appear to be useful in covalent systems and have not been considered in previous work. The energies of the $\Sigma5$ and $\Sigma5^*$ boundaries are similar and around 6 eV/unit-cell. This implies the possible existence

of structural domains and even structural multiplicity as described in the previous sections.

Since our density-functional calculations were performed using rapid quenches, our results are relevant to experiments at least at very short time scales. Under these conditions, one would expect to find a wealth of metastable states having similar energy. Tunneling between them should be possible by ammonia-like inversions, bond-switching reactions, and exchanges of vacancies and interstitials. As one allows the system to anneal further, it will gradually find deeper and deeper energy minima (if they exist) using larger distortions. There will be fewer metastable states, tunneling between them will be less frequent, and atoms further away from the boundary will be displaced.

Finally, the bonding characteristics of the twist boundaries and their effect on the local electronic structure appear to be quite different from well-coordinated tilt boundary structures. In symmetric-tilt boundary calculations,[46] it has been found that structures containing no broken bonds can be found relatively easily and that the energy-translation surface exhibits a well-defined energy minimum. It is proposed that this difference in structural characteristics is universal among covalently bonded solids and may be attributed to the different degrees of frustration associated with the two types of boundary. The frustration results from the tendency to maintain local directional bonding, both across the grain boundary and into the bulk. For the tilt orientation, this frustration may be thought of as one dimensional, while for the twist orientation, it is two dimensional. The higher level of disorder in the twist boundary leads to a variety of bond distortions and the appearance of electronic states deep in the band gap as can be seen in Fig. 19. This is in sharp contrast to recent tight-binding results[17] on the $\Sigma 5(310)$ tilt boundary in silicon, where only shallow states associated with the upper edge of the valence band and the lower edge of the conduction band were found.

ACKNOWLEDGMENTS

The authors are grateful to the following agencies for support: U.S. Air Force Office of Scientific Research (ET and JDJ, under Grant No. AFOSR-90-0276 U.S. Department of Energy (PDB, under Grant No. DE-FG02-87ER45310), United Kingdom Science and Engineering Research Council (G. P. F. and M. C. P., under Grant No. GR/E/25948), and the French Délégation Générale pour l'Armement (P.D.). Supercomputer time was provided by the National Science Foundation at the Pittsburgh Supercomputing Center.

*Present address: Xerox Corporation, Palo Alto Research Center, 3333 Coyote Hill Road, Palo Alto, CA 94304.

[1]See articles in J. Phys. (Paris) Colloq. **46**, C-4 (1985).

[2]See articles in *Interfaces, Superlattices, and Thin Films,* Vol. 77 of *Materials Research Society Symposium Proceedings,* edited by J. D. Dow and I. K. Schuller (MRS, Pittsburgh, 1987).

[3]R. W. Balluffi and P. D. Bristowe, Surf. Sci. **144**, 28 (1984).

[4]P. D. Bristowe and R. W. Balluffi, J. Phys. (Paris) Colloq. **46**, C4-155 (1985).

[5]D. Wolf and S. Phillpot, Mater. Sci. Eng. A **107**, 3 (1989).

[6]I. Majid, P. D. Bristowe, and R. W. Balluffi, Phys. Rev. B **40**, 2779 (1989).

[7]A. Bourret and J. J. Bacmann, Rev. Phys. Appl. **22**, 563 (1987).

[8]M. C. Payne, P. D. Bristowe, and J. D. Joannopoulos, Phys. Rev. Lett. **58**, 1348 (1987).

[9]A. T. Paxton and A. P. Sutton, Acta Metall. **37**, 1693 (1989).

[10]R. Car and M. Parrinello, Phys. Rev. Lett. **55**, 2471 (1985).

[11]M. C. Payne, J. D. Joannopoulos, D. C. Allan, M. P. Teter, and D. H. Vanderbilt, Phys. Rev. Lett. **56**, 2656 (1986).

[12]J. D. Joannopoulos, in *Physics of Disordered Materials,* edited by D. Adler, H. Fritzsche, and S. R. Ovshinsky (Plenum, New York, 1985), p. 19.

[13]R. E. Thomson and D. J. Chadi, Phys. Rev. B **29**, 889 (1984).

[14]D. P. DiVincenzo, O. L. Alerhand, M. Schluter, and J. W. Wilkins, Phys. Rev. Lett. **56**, 1925 (1986).

[15]A. Mauger, J. C. Bourgoin, G. Allan, M. Lannoo, A. Bourret, and L. Billard, Phys. Rev. B **35**, 1267 (1987).

[16]M. Kohyama, R. Yamamoto, and M. Doyama, Phys. Status Solidi B **137**, 11 (1986); B **138**, 387 (1986).

[17]M. Kohyama, R. Yamamoto, Y. Ebata, and M. Kinoshita, J. Phys. C **21**, 3205 (1988).

[18]M. Kohyama, R. Yamamoto, Y. Watanabe, Y. Ebata, and M. Kinoshita, J. Phys. C **21**, L695 (1988).

[19]A. T. Paxton and A. P. Sutton, J. Phys. C **21**, L481 (1988).

[20]M. Kohyama, R. Yamamoto, and M. Doyama, Phys. Status Solidi B **136**, 31 (1986).

[21]D. Wolf, J. Phys. (Paris) Colloq. **46**, C4-197 (1985).

[22]S. R. Phillpot and D. Wolf, Philos. Mag. A **60**, 545 (1989).

[23]A. Bourret, J. Phys. (Paris) Colloq. **46**, C4-27 (1985).

[24]E. Tarnow, P. D. Bristowe, J. D. Joannopoulos, and M. C. Payne, J. Phys. Condens. Matter **1**, 327 (1989).

[25]References 8 and 24 present results using a Fourier-transform box that was too small. Moreover, Ref. 8 did not include corrections for the Pulay force. These errors lead to energy differences which are correct for the unrelaxed structures but incorrect for the relaxed structures. The atomic configurations of each geometry, however, remain very similar.

[26]W. Mader, C. Necker, and R. W. Balluffi, J. Phys. (Paris) Colloq. **49**, C5-233 (1988).

[27]J. J. Bacmann, G. Silvestre, M. Petit, and W. Bollmann, Philos. Mag. A **43**, 189 (1981).

[28]M. Vaudin and D. Ast, in *Defects in Semiconductors II,* Vol. 14 of *Materials Research Society Symposium Proceedings,* edited by S. Mahajan and J. W. Corbett (MRS, Pittsburgh, 1983), p. 369.

[29]C. R. M. Grovenor, J. Phys. C **18**, 4079 (1985).

[30]See papers in J. Phys. (Paris) Colloq. **49**, C5 (1988).

[31]See papers in *Polycrystalline Semiconductors,* Vol. 35 of *Springer Proceedings in Physics,* edited by H. J. Möller, H. P. Strunk, and J. H. Werner (Springer, Berlin, 1989).

[32]W. Bollmann, *Crystal Defects and Crystalline Interfaces* (Springer, Berlin, 1970).

[33]R. C. Pond and D. S. Vlachavas, Proc. R. Soc. London, Ser. A **386**, 95 (1983).

[34]R. C. Pond, in *Microscopy of Semiconducting Materials,* Inst. Phys. Conf. Ser. No. 67 (IOP, London, 1983), p. 59.

[35]P. Perdew and A. Zunger, Phys. Rev. B **16**, 5188 (1976).

[36]Th. Starkloff and J. D. Joannopoulos, Phys. Rev. B **16**, 5212 (1977).
[37]P. Pulay, Mol. Phys. **17**, 197 (1969); J. Geratt and I. M. Mills, J. Chem. Phys. **49**, 1719 (1968).
[38]All energies are quoted with respect to bulk Ge.
[39]M. C. Payne, P. D. Bristowe, and J. D. Joannopoulos, J. Phys. (Paris) Colloq. **49**, C5-151 (1988).
[40]M. C. Payne, N. Roberts, R. J. Needs, M. Needels, and J. D. Joannopoulos, Surf. Sci. **211/212**, 1 (1989).
[41]G. Etherington, A. C. Wright, J. T. Wenzel, J. C. Doie, J. H. Clark, and R. N. Sinclair, J. Non-Cryst. Solids **48**, 265 (1982).
[42]J.-L. Maurice, Rev. Phys. Appl. **22**, 613 (1987).
[43]A. M. Papon and M. Petit, Scr. Metall. **19**, 391 (1985).
[44]A. Bourret and J. L. Rouviere, in *Polycrystalline Semiconductors,* Vol. 35 of *Springer Proceedings in Physics,* edited by H. J. Möller, H. P. Strunk, and J. H. Werner (Springer, Berlin, 1989), p. 8.
[45]F. H. Stillinger and T. A. Weber, Phys. Rev. B **31**, 5262 (1985).
[46]T. Arias and J. D. Joannopoulos (unpublished).

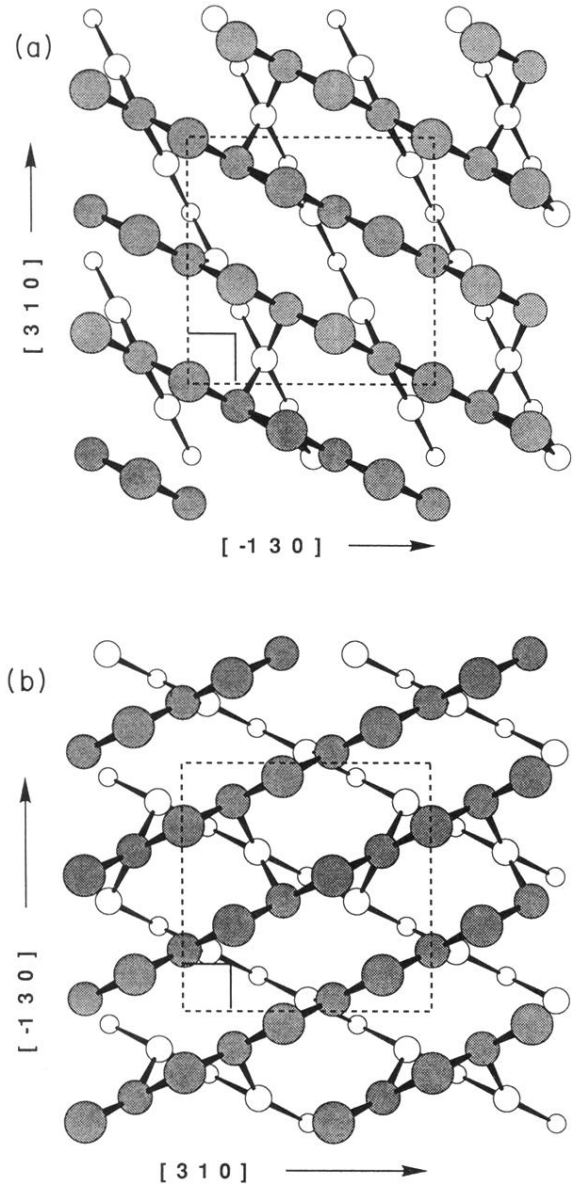

FIG. 1. Unrelaxed atomic positions in planes normal to the [001] direction for two twist boundaries in germanium: (a) $\Sigma 5(36.9°)$ and (b) $\Sigma 5^*(53.1°)$. Two layers above (solid circles) and below (open circles) the boundary plane are shown in both cases. The CSL unit cell is indicated by dashed lines and the smaller DSC cell is indicated by solid lines. Note that the x and y directions are reversed in (a) and (b), and that there is no relative translation of the upper and lower layers.

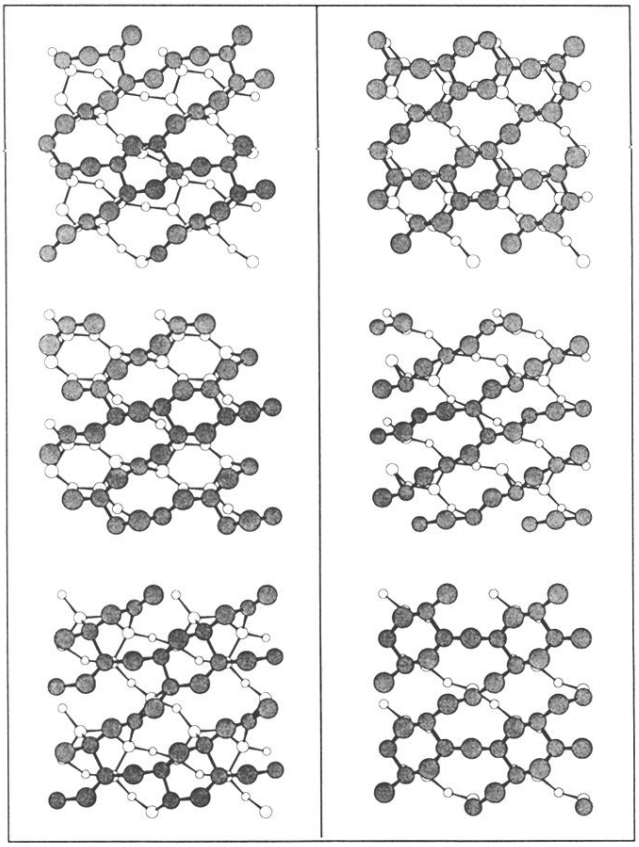

FIG. 15. Relaxed atomic configurations corresponding to the energy extrema $A-F$ in Fig. 14. The three minima A, B, and C, and the three maxima D, E, and F are shown top to bottom in the left- and right-hand panels, respectively.

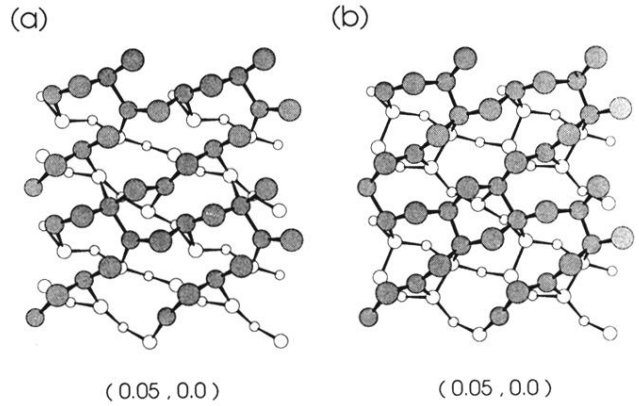

FIG. 16. Two relaxed atomic configurations of the (0.05,0) or the $\frac{1}{40}a[310]$ state of $\Sigma 5^*$. (a) was obtained from relaxation of the rigid-body geometry and (b) was obtained by translating the relaxed (0,0) state to (0.05,0) and rerelaxing.

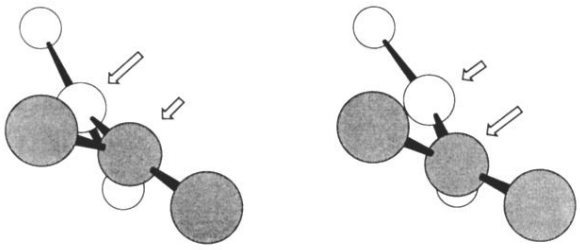

FIG. 18. Characteristic group of atoms that form part of two different translation states of $\Sigma 5$ that are symmetry equivalent, but yield different configurations. The arrows highlight the differences.

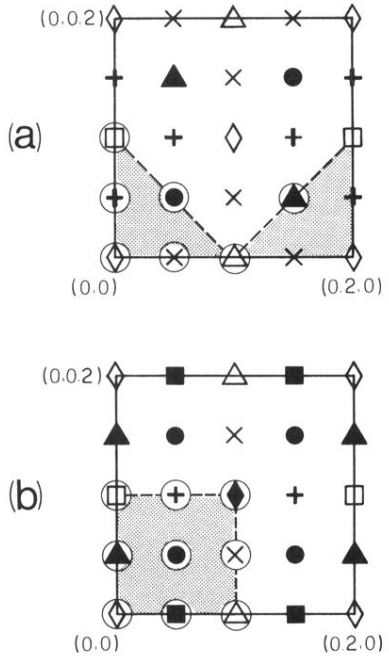

FIG. 2. DSC unit cells (solid lines) for (a) $\Sigma 5(36.9°)$ boundary and (b) $\Sigma 5^*(53.1°)$ boundary. The shaded areas indicated the irreducible zones for both boundaries. The coordinates are given as fractions of a CSL vector. Note that the x and y directions are reversed in (a) and (b) to be consistent with Fig. 1. The different symbols indicate symmetry-related positions and the circled symbols refer to structures that were computed.

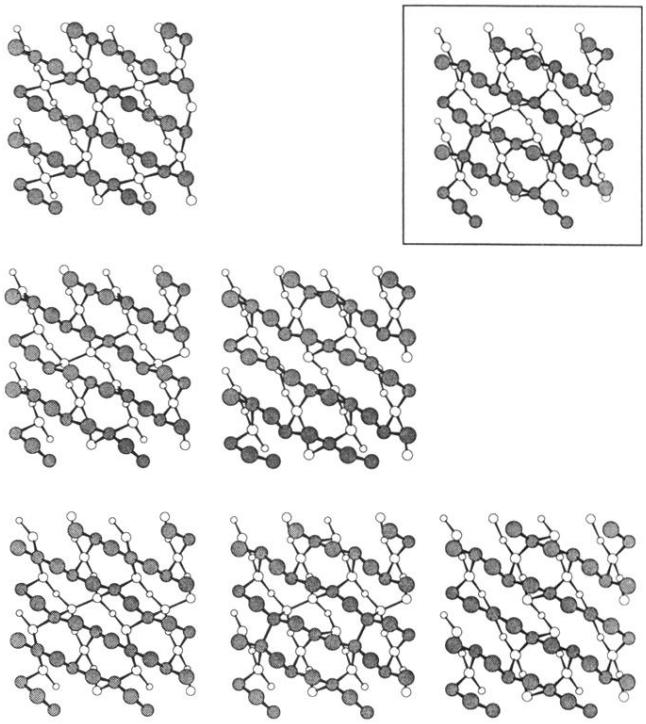

FIG. 8. Relaxed atomic configurations of the seven translation states of $\Sigma 5$ (36.9°). The orientation of the structures is the same as in Fig. 1(a). Their arrangement in the figure corresponds directly to the arrangement of circled symbols in Fig. 2(a) with the exception of the boxed structure, which corresponds to the state (0.15,0.05). Thus, the (0,0) state is the structure in the lower left-hand corner.

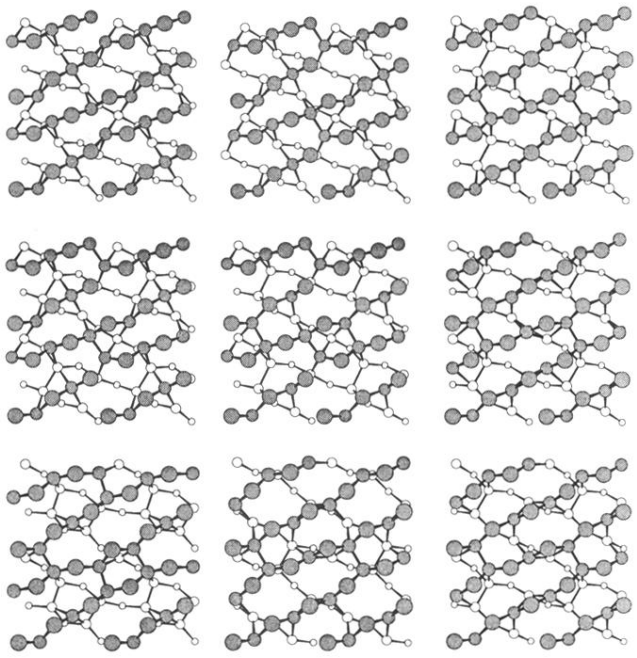

FIG. 9. Relaxed atomic configurations of the nine translation states of $\Sigma 5^*$ (53.1°). The orientation of the structures is the same as in Fig. 1(b). Their arrangement in the figure corresponds directly to the arrangement of circled symbols in Fig. 2(b). Thus the (0,0) state, which has the lowest energy, is the structure in the lower left-hand corner.